Electronic Supplementary Information (ESI)

Copper(I) and cobalt(II) frameworks with a tetraphenylethene-imidazole ligand for electroreduction CO_2 to CH_4

Fang-Fang Wang, Yu-Jie Wang, Zhao-Feng Qiu, Kai-Yang Zhang, Yue Zhao and Wei-Yin Sun*

Coordination Chemistry Institute, State Key Laboratory of Coordination Chemistry, School of Chemistry and Chemical Engineering, Nanjing National Laboratory of Microstructures, Collaborative Innovation Center of Advanced Microstructures, Nanjing University, Nanjing 210023, China

* Corresponding author.

Email address: sunwy@nju.edu.cn (W. Y. Sun)

Physical measurements

Powder X-ray diffraction patterns (PXRD) of the samples were measured on the Bruker D8 Advance X-ray diffractometer using Cu-Kα (λ = 1.5418 Å) radiation. The voltage of the instrument was 40 kV, the current was 40 mA. The total reflection infrared (ATR-IR) spectra of the samples were obtained using a Fourier transform infrared (FTIR) spectrometer (TENSOR 27) with a spectral range of 4000 - 400 cm^{-1}. Thermalgravimetric analysis (TGA) was conducted on the Mettler-Toledo (TGA/DSC1) thermal analyzer, and TGA was performed under N_2 at a heating rate of 10 °C min^{-1}. The elemental content of the samples was determined by the Elementar UNICUBE element analyzer. X-ray photoelectron spectroscopy (XPS) was performed on ThermoFisher Nexsa with aluminum Al radiation.

Working electrode preparation

A homogenous ink was formed by sonicating 950 μL of isopropanol solution with 10 mg of

catalyst and 50 μL of Nafion solution (5 wt%) for 0.5 h. Subsequently, 200 μL of the uniform ink dispersion was transferred onto a 1 x 1 cm^2 carbon paper (CP) electrode and allowed to dry in the ambient environment.

Electrochemical test

Electrocatalytic CO_2RR tests were performed using a three-channel flow cell on the electrochemical workstation (CHI 730E, Chenhua, Shanghai). Electrochemical impedance spectroscopy (EIS) was performed on the Zahner electrochemical workstation (IM6ex, Zahner Scientific Instruments, German). Cyclic voltammetry (CV) profiles and linear sweep voltammetry (LSV) curves were measured at a sweep rate of 100 mV s^{-1} with N_2/CO_2. All potentials in this work were converted to reversible hydrogen electrodes (RHE) using the Nernst equation: $E_{RHE} = E_{Hg/HgO} + 0.098 + 0.059 \times pH$.

Product quantification

An online gas chromatograph was used for the separation and identification of the components of a gas mixture. The potential products (H_2, CH_4, CO, C_2H_4) emerging from the outlet of the cathodic compartment were directly vented into the gas chromatograph system (GC9790II, Fuli), which was equipped with a thermal conductivity detector (TCD) and flame ionization detector (FID) with a methaniser. The gas chromatograph was equipped with a Molecular Sieve 5A column, a Popapak N column, and a Haysep4 column. Argon (Tianhong Gas, 99.999%) was used as the carrier gas, with a GC run initiated every 18 min. High-purity Ar (99.999%) was used as the carrier gas.

^1H NMR spectra were collected on a Bruker DRX 500 MHz spectrometer. The NMR samples were prepared by mixing 0.4 mL of electrolyte with 0.05 μL of deuterated water (D_2O), and 0.05 μL of dimethyl sulfoxide (DMSO) was added as an internal standard. The pre-saturation method was employed to eliminate the water peak.

Calculations of product and Faradaic efficiency (FE)

$$FE_{gas} = \frac{n \times F \times P \times V_{gas} \times q_{gas}}{i \times R \times T} \times 100\%$$

$$FE_{liquid} = \frac{n \times c \times V_{liquid} \times F}{Q} \times 100\%$$

In this equation, n represents the number of electrons transferred to the specific product, which is 2 for formic acid. F is the Faraday constant (96500 C mol^{-1}), P = 1.01 × 105 Pa, V_{gas} is the volume fraction of the gas product, and q_{gas} is the gas flow rate. Finally, i(A) is the total current density at each applied potential, R = 8. 314 J mol^{-1} K^{-1}, T = 298.15 K, c representing the molar concentration of liquid products, V_{liquid} the volume of cathode electrolyte, and Q (C) the total amount of applied electricity.

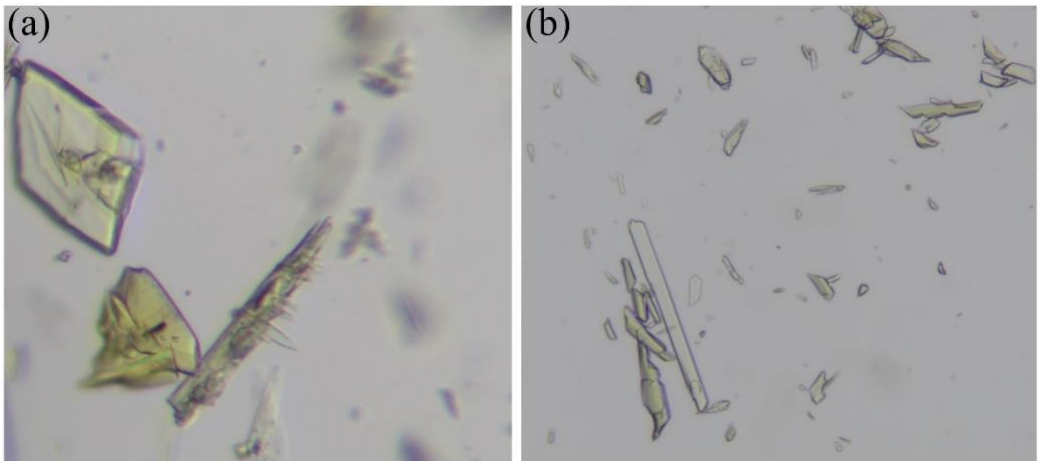

Figure S1. The optical images of **Cu-MOF** (a) and **Co-MOF** (b).

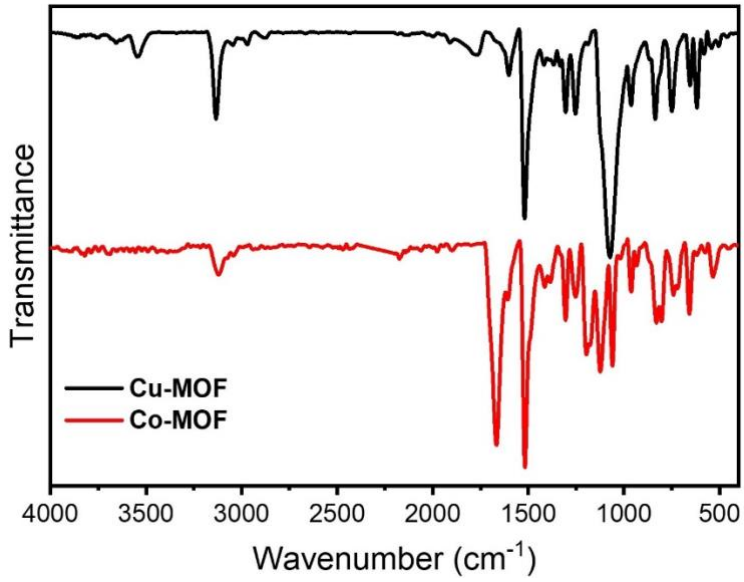

Figure S2. FT-IR spectra of **Cu-MOF** and **Co-MOF**.

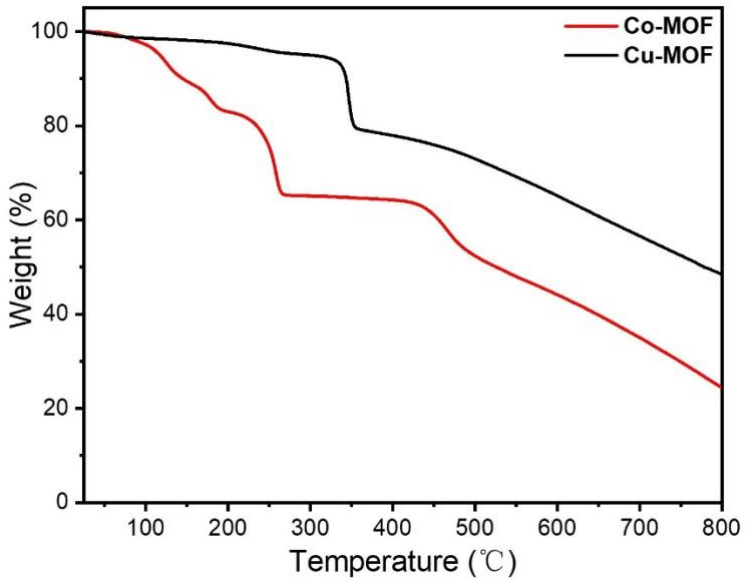

Figure S3. TG curves of **Cu-MOF** and **Co-MOF**.

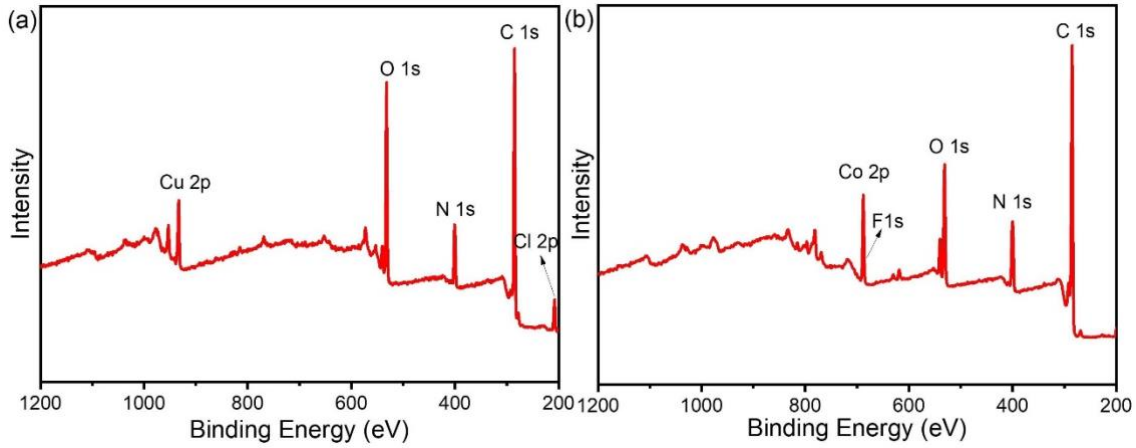

Figure S4. XPS survey spectra of (a) **Cu-MOF** and **Co-MOF**.

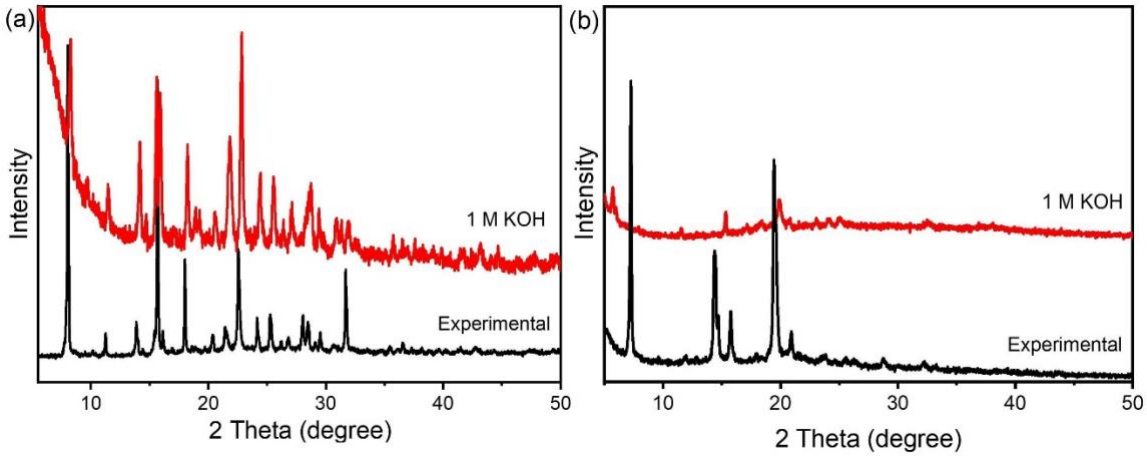

Figure S5. PXRD patterns of **Cu-MOF** (a) and **Co-MOF** (b) after immersing in 1 M KOH for 24 h.

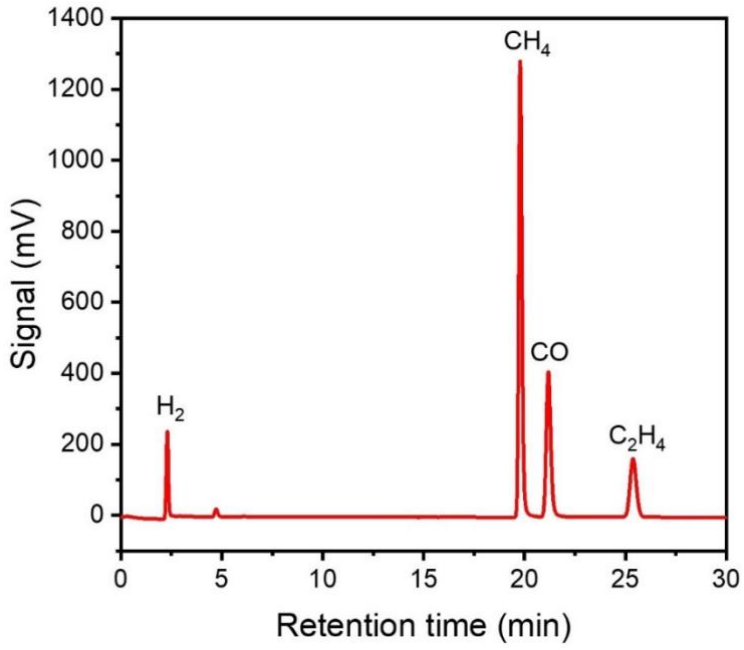

Figure S6. Online GC analysis results of **Cu-MOF** at an applied potential of -1.28 V (vs. RHE).

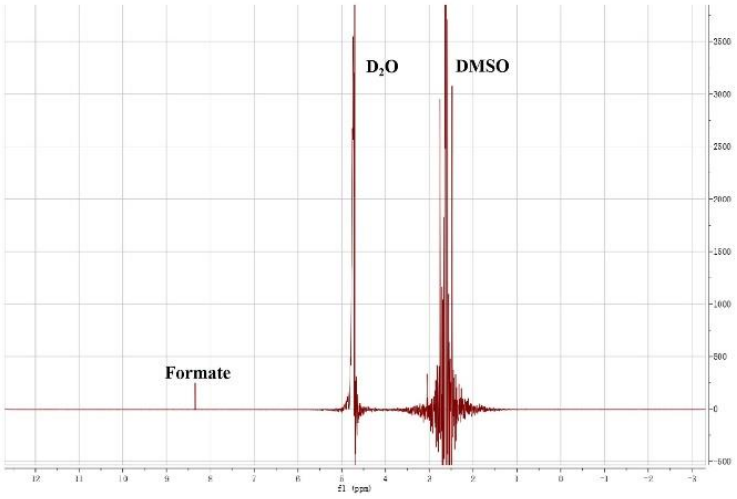

Figure S7. ^{1}H NMR spectrum of the electrolyte after CO_2RR.

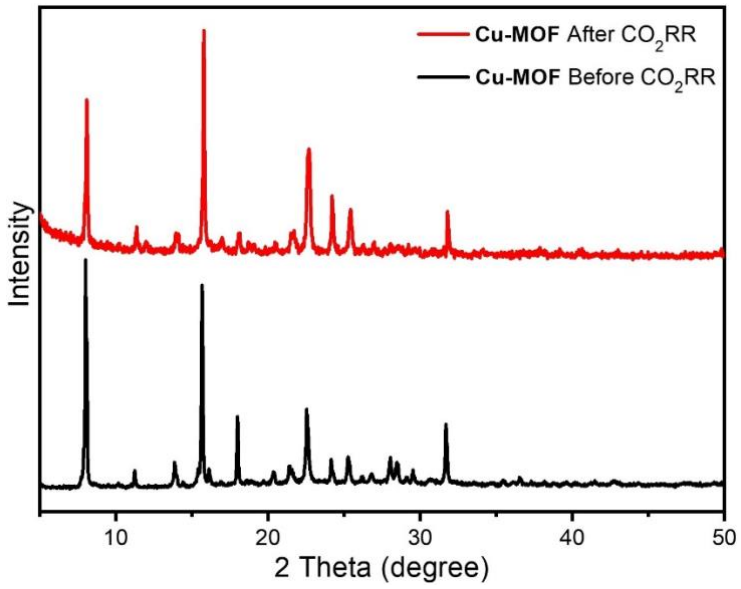

Figure S8. PXRD patterns of **Cu-MOF** before and after CO_2RR test.

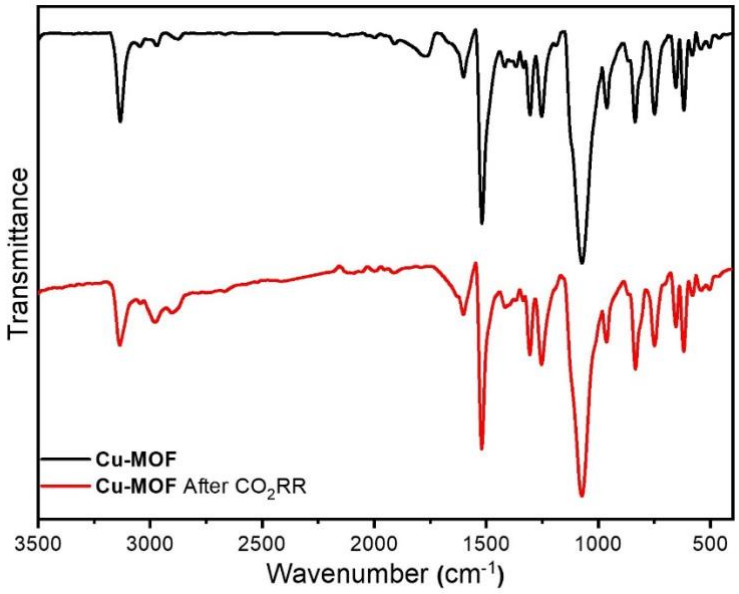

Figure S9. FT-IR spectra of **Cu-MOF** before and after the CO_2RR test.

Table S1. Selected bond lengths (Å) and angles (°) for **Cu-MOF**.

Cu-MOF			
Cu(1)-N(1)	1.872(5)	Cu(1)-N(3)#1	1.877(6)
N3#1-Cu(1)-N(1)	177.2(3)		

Symmetry transformations used to generate equivalent atoms:

#1 -3/2+X, -1/2+Y, -1+Z

Table S2. Selected bond lengths (Å) and angles (°) for **Co-MOF**.

Co-MOF			
Co(1)-N(1)	2.127(3)	Co(1)-O(3)	2.146(3)
Co(1)-N(4)#1	2.140(3)	Co(1)-N(6)#2	2.156(3)
Co(1)-N(8)#3	2.125(3)	Co(1)-O(1)	2.120(5)
O(1)-Co(1)-N(8)#3	90.8(3)	N(1)-Co(1)-O(3)	94.19(11)
N(1)-Co(1)-N(4)#1	86.95(12)	N(1)-Co(1)-N(6)#2	86.21(12)
O(3)-Co(1)-N(6)#2	84.49(11)	N(4)#1-Co(1)-O(3)	93.44(12)
N(4)#1-Co(1)-N(6)#2	172.69(11)	N(8)#3-Co(1)-N(1)	176.34(13)
N(8)#3-Co(1)-O(3)	87.55(11)	N(8)#3-Co(1)-N(4)#1	96.17(12)
N(8)#3-Co(1)-N(6)#2	90.75(11)	O(1)-Co(1)-N(1)	87.4(3)
O(1)-Co(1)-O(3)	178.0(3)	O(1)-Co(1)-N(4)#1	87.9(3)
O(1)-Co(1)-N(6)#2	94.3(3)		

Symmetry transformations used to generate equivalent atoms:

#1 -1+X, +Y, +Z; #2 +X, 1+Y, 1+Z; #3 -1+X, 1+Y, +Z.

Table S3. Analysis of π···π and C-H···π interactions in **Cu-MOF**.

CgI→CgJ	Cg-Cg (Å)	CgI→CgJ	Cg-Cg (Å)
Cg1→Cg1#1	3.526(4)	Cg2→Cg2#2	3.922(4)
C-H→Cg(I)	H···Cg (Å)	C-H→Cg(I)	H···Cg (Å)
C9-H9→Cg4#3	2.88	C13-H13→Cg1#4	2.89

Symmetry codes: #1 -x, y, -z; #2 2-x, y, 2-z; #3 -1/2+x, -1/2+y, z; #4 1/2-x, 1/2+y, 1-z. CgI: the conjugated rings number in **Cu-MOF**; Cg-Cg: distance between ring centroids; H···Cg: distance of hydrogen atoms to ring centroid; H-Perp: perpendicular distance of H to ring plane I; C..Cg: distance of carbon atoms to ring centroid; X-H···Cg: X-H-Cg angle. Cg1: N1→C1→C2→N2→C3; Cg2: N3→C19→C18→N4→C20; Cg3: C4→C5→C6→C7→C8→C9; Cg4: C12→C13→C14→C15→C16→C17.

Table S4. Analysis of π···π interactions in **Co-MOF**.

CgI→CgJ	Cg-Cg (Å)
Cg1→Cg2#1	4.805(3)

Symmetry codes: #1 3/2-x, -1/2+y, 1/2-z. CgI: the conjugated rings number in **Co-MOF**; Cg-Cg: distance between ring centroids; Cg: distance of carbon atoms to ring centroid; Cg1: C21→C22→C23→C24→C25→C26; Cg2: N3→C17→N4→C18→C19.

Table S5. Comparison of the selectivity and partial current density of CH_4 production with reported catalysts.

Catalysts	Electrolyte	FE_{CH4} (%)	Partial current density of CH_4 (mA cm^{-2})	Ref.
Cu@Al-fum MOF	0.1 M $KHCO_3$	6	7	1
Cu–Zn@Al-fum MOF	0.1 M $KHCO_3$	16	5	1
Cu_2O-QDs@CuHHTPMOF	0.1MKCl/0.1M $KHCO_3$	73	10.8	2
Cu-DBC	0.1 M $KHCO_3$	56	11.4	3
Co-MOF-525	0.1 M $LiClO_4$ and 11M Double-distilled water	14	<10	4
HKUST-1 + CNT	0.5 M $KHCO_3$	4.4	27	5
HKUST-1 on a (GDE)	1 M KOH	15	10	6
Crystalline CuPc	0.5 M KCl	4	0.5	7
Cu NPs with 15 wt% $Cu_3(BTC)_2$	0.5 M $NaHCO_3$	20	4.5	8
Cu-MOF	**1 M KOH**	**41.5**	**38.95**	**This work**

Reference

1 U. T. Dieu Thuy, T. N. Huan, S. Zanna, K. Wilson, A. F. Lee, N. D. Le, J. Mensah, V. D. B. C. Dasireddy and N. Q. Liem, *RSC Adv.*, 2024, **14**, 3489–3497.

2 Y. T. Guntern, J. R. Pankhurst, J. Vávra, M. Mensi, V. Mantella, P. Schouwink and R.

Buonsanti, *Angew. Chem. Int. Ed.*, 2019, **58**, 12632–12639.

3 Y. Y. Liu, H. L. Zhu, Z. H. Zhao, N. Y. Huang, P. Q. Liao and X. M. Chen, *ACS Catal.*, 2022, **12**, 2749–2755.

4 R. Ifraemov, S. Mukhopadhyay and I. Hod, *Sol. RRL*, 2023, **7**, 2201068.

5 Z. Weng, Y. Wu, M. Wang, J. Jiang, K. Yang, S. Huo, X. F. Wang, Q. Ma, G. W. Brudvig, V. S. Batista, Y. Liang, Z. Feng and H. Wang, *Nat. Commun.*, 2018, **9**, 415.

6 J. Albo, D. Vallejo, G. Beobide, O. Castillo, P. Castaño and A. Irabien, *ChemSusChem*, 2017, **10**, 1100–1109.

7 S. Kusama, T. Saito, H. Hashiba, A. Sakai and S. Yotsuhashi, *ACS Catal.*, 2017, **7**, 8382–8385.

8 Y. L. Qiu, H. X. Zhong, T. T. Zhang, W. Bin Xu, P. P. Su, X. F. Li and H. M. Zhang, *ACS Appl. Mater. Interfaces*, 2018, **10**, 2480–2489.